J Eng Math (2012) 75:49–62
DOI 10.1007/s10665-011-9512-2

On rimming flows with shocks

E. S. Benilov · V. N. Lapin · S. B. G. O'Brien

Received: 28 April 2011 / Accepted: 13 September 2011 / Published online: 22 November 2011

Abstract We examine rimming flows, i.e. flows of a liquid film on the inside of a horizontal rotating cylinder. So far this problem has mostly been explored using the so-called lubrication approximation (LA). It was shown that, if the volume of the liquid in the cylinder exceeds a certain threshold, then a shock similar to a tidal bore appears in the lower half of the cylinder on its rising side. The position of the shock can be characterized by the polar angle θ_s, with a value between $\theta_s = -90°$ (the bottom of the cylinder) and $\theta_s = 0°$ (the horizontal direction). In this study, we examine rimming flows without the LA, by solving numerically the exact Stokes equations. It is shown that a steady solution describing a (smoothed) shock exists only if $-60° \lesssim \theta_s < 0°$. Shocks with lower locations overturn, so no steady solution exists. It is also shown that smoothed-shock solutions have an oscillating structure upstream from the shock. If, however, capillary effects are taken into account, the range of θ_s where solutions overturn contracts, and if surface tension is sufficiently strong, solutions exist for all values of θ_s.

Keywords Liquid films · Rimming flows · Wave overturning

1 Introduction

Rimming flows, i.e. flows of a liquid film on the inside of a rotating horizontal cylinder, have important industrial applications and are also of significant interest to a theoretician. They were first examined by Moffatt [1] using the so-called lubrication approximation (LA), i.e. an assumption that the film is thin, the Reynolds number is small, and so is the slope of the film surface relative to the cylinder wall. Assuming also that surface tension is negligible and the flow is uniform in the direction of the cylinder axis, Moffatt demonstrated that, if the volume V of the liquid does not exceed a certain threshold V_1, the liquid is fully entrained by the cylinder rotation and is spread smoothly over its surface (see Fig. 1a). If, however, $V = V_1$, then a corner appears in the profile of the flow (see Fig. 1b). Using the same model, [2,3] examined the case $V > V_1$ and showed that a shock similar to a tidal bore forms in the lower half of the cylinder, on its rising side (see Fig. 1c).

E. S. Benilov (✉) · V. N. Lapin · S. B. G. O'Brien
MACSI, Department of Mathematics, University of Limerick, Limerick, Ireland
e-mail: eugene.benilov@ul.ie

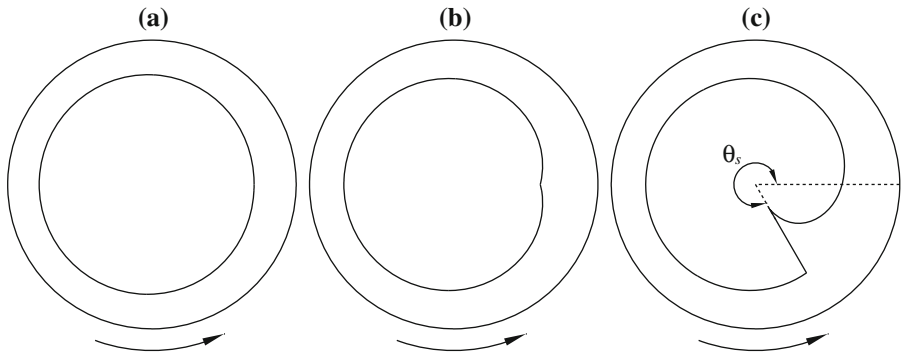

Fig. 1 A schematic illustrating types of rimming flows: **a** smooth flow, **b** flow with a corner, **c** flow with a shock

Note, however, that the discontinuity of shock solutions is an artifact introduced by the omission of surface tension and non-lubrication effects[1] from the model—if present, either would smooth the discontinuity. To remedy this problem, surface tension was introduced to the model and its effect on the shock solutions was studied in [4,5]. Non-lubrication effects, in turn, were explored in [6,7] using phenomenological models.

Note also that, in addition to V_1, there is another threshold $V_2 > V_1$: if the liquid volume exceeds V_2, the shock cannot hold on to the rising side of the cylinder, and the liquid pools at the cylinder bottom. Unlike the smooth and shock solutions, those with pools do not satisfy Moffatt's model [1] as they are crucially affected by non-lubrication effects and/or surface tension. The latter has been examined in [4,8] and the former, in [6,7]. Note also that smoothing of the corner solution (shown in Fig. 1b) by the non-lubrication effects has been examined by Wilson et al. [9], and non-stationary shock-like solutions smoothed by surface tension have been examined in [10].

In this article, we shall re-examine how the shock solutions are affected by the non-lubrication effects (the corner and pool solutions will not be discussed). Unlike [6,7], we shall explore the structure of shock waves through direct numerical simulations. We shall also discuss how they are affected by surface tension.

2 Formulation

Consider a thin film of liquid (of density ρ, kinematic viscosity ν, and surface tension σ) on the inside of a cylinder of radius R with a horizontal axis, rotating about this axis with a constant angular velocity Ω. The problem also involves the acceleration due to gravity, g, so three dimensionless parameters can be introduced, say,

$$\varepsilon = \frac{R\Omega^2}{g}, \qquad \gamma = \frac{\sigma}{\rho\nu\Omega R}, \qquad \alpha = \left(\frac{\nu\Omega}{gR}\right)^{1/2}, \tag{1}$$

where ε is the ratio of the centrifugal force to gravity, γ is the dimensionless capillary coefficient, and the parameter α was shown by Benjamin et al. [2] to represent the ratio of the characteristic film thickness in a shock solution to the cylinder radius R.

2.1 The governing equations

We are concerned with two-dimensional flows, depending on the time t_* (asterisks denote dimensional variables) and polar coordinates (r_*, θ_*) where $\theta_* = 0$ corresponds to the horizontal. We shall also introduce the radial and azimuthal velocities, v_* and u_*, pressure p_*, and the film thickness h_*.

[1] Here and hereinafter, the effects associated with the slope of the free surface being finite (as opposed to infinitesimal) will be referred to as non-lubrication effects.

The following dimensionless variables will be used:

$$y = \frac{R - r_*}{\alpha R}, \qquad \theta = \theta_*, \qquad t = \Omega t_*, \tag{2}$$

$$v = -\frac{v_*}{\alpha R \Omega}, \qquad u = \frac{u_*}{R\Omega}, \qquad p = \frac{\alpha p_*}{\rho \nu \Omega}, \qquad h = \frac{h_*}{\alpha R} \tag{3}$$

(observe the minus in the expression for the radial velocity v, matching the minus in the expression for the radial coordinate y). In terms of variables (2–3), the Navier–Stokes equations are

$$\varepsilon\left[\alpha\frac{\partial v}{\partial t} + \alpha v\frac{\partial v}{\partial y} + \frac{u}{1-\alpha y}\left(\alpha\frac{\partial v}{\partial \theta} + u\right)\right] + \frac{\partial p}{\partial y} = \sin\theta$$
$$+\alpha\left[\frac{\partial^2 v}{\partial y^2} - \frac{\alpha}{1-\alpha y}\frac{\partial v}{\partial y} + \frac{\alpha}{(1-\alpha y)^2}\left(\alpha\frac{\partial^2 v}{\partial \theta^2} - \alpha v + 2\frac{\partial u}{\partial \theta}\right)\right], \tag{4}$$

$$\varepsilon\left[\frac{\partial u}{\partial t} + v\frac{\partial u}{\partial y} + \frac{u}{1-\alpha y}\left(\frac{\partial u}{\partial \theta} - \alpha v\right)\right] + \frac{\alpha}{1-\alpha y}\frac{\partial p}{\partial \theta} = -\cos\theta$$
$$+\frac{\partial^2 u}{\partial y^2} - \frac{\alpha}{1-\alpha y}\frac{\partial u}{\partial y} + \frac{\alpha^2}{(1-\alpha y)^2}\left(\frac{\partial^2 u}{\partial \theta^2} - u - 2\alpha\frac{\partial v}{\partial \theta}\right), \tag{5}$$

$$(1-\alpha y)\frac{\partial v}{\partial y} - \alpha v + \frac{\partial u}{\partial \theta} = 0. \tag{6}$$

The no-normal-velocity and no-slip conditions at the cylinder wall are

$$v = 0, \qquad u = 1 \qquad \text{at } y = 0. \tag{7}$$

The following standard boundary conditions will be imposed at the free surface,

$$\mathbf{n}^{\mathrm{T}}\mathbf{S}\mathbf{n} = \gamma\alpha^2 C, \qquad \boldsymbol{\tau}^{\mathrm{T}}\mathbf{S}\mathbf{n} = 0 \qquad \text{at } y = h, \tag{8}$$

where

$$\mathbf{n} = \frac{1}{\sqrt{1 + \left(\frac{\alpha}{1-\alpha h}\frac{\partial h}{\partial \theta}\right)^2}}\begin{bmatrix} 1 \\ \frac{\alpha}{1-\alpha h}\frac{\partial h}{\partial \theta} \end{bmatrix}, \qquad \boldsymbol{\tau} = \begin{bmatrix} \frac{\alpha}{1-\alpha h}\frac{\partial h}{\partial \theta} \\ -1 \end{bmatrix} \tag{9}$$

are the unit normal vector and a tangent vector (not necessarily unit) to the free surface, the superscript $^{\mathrm{T}}$ denotes matrix transposition,

$$\mathbf{S} = \begin{bmatrix} 2\alpha\frac{\partial v}{\partial y} - p & -\frac{\alpha}{1-\alpha h}\left(\alpha\frac{\partial v}{\partial \theta} + u\right) - \frac{\partial u}{\partial y} \\ -\frac{\alpha}{1-\alpha h}\left(\alpha\frac{\partial v}{\partial \theta} + u\right) - \frac{\partial u}{\partial y} & \frac{2\alpha}{1-\alpha h}\left(\frac{\partial u}{\partial \theta} - \alpha v\right) - p \end{bmatrix} \tag{10}$$

is the stress tensor, and

$$C = \frac{(1-\alpha h)^2 + \alpha\,(1-\alpha h)\,\frac{\partial^2 h}{\partial \theta^2} + 2\alpha^2\left(\frac{\partial h}{\partial \theta}\right)^2}{\alpha\left[(1-\alpha h)^2 + \alpha^2\left(\frac{\partial h}{\partial \theta}\right)^2\right]^{3/2}} \tag{11}$$

is the dimensionless curvature of the free surface. The scalar conditions (8) can be re-written in the form of a single vector condition,

$$\left(\mathbf{S} - \gamma\alpha^2 C\mathbf{I}\right)\mathbf{n} = \mathbf{0} \qquad \text{at } y = h, \tag{12}$$

where $\mathbf{I}$ is the unit matrix. Substituting (9–10) into (12), we obtain

$$2\alpha\frac{\partial v}{\partial y} - p - \gamma\alpha^2 C - \left[\frac{\alpha}{1-\alpha h}\left(\alpha\frac{\partial v}{\partial\theta} + u\right) + \frac{\partial u}{\partial y}\right]\frac{\alpha}{1-\alpha h}\frac{\partial h}{\partial\theta} = 0 \quad \text{at } y = h, \tag{13}$$

$$\frac{\alpha}{1-\alpha y}\left(\alpha\frac{\partial v}{\partial\theta} + u\right) + \frac{\partial u}{\partial y} - \left[\frac{2\alpha}{1-\alpha h}\left(\frac{\partial u}{\partial\theta} - \alpha v\right) - p - \gamma\alpha^2 C\right]\frac{\alpha}{1-\alpha h}\frac{\partial h}{\partial\theta} = 0 \quad \text{at } y = h. \tag{14}$$

Finally, we shall impose the kinematic condition at the free surface,

$$\frac{\partial h}{\partial t} + \frac{u}{1-\alpha h}\frac{\partial h}{\partial\theta} - v = 0 \quad \text{at } y = h. \tag{15}$$

2.2 The lubrication approximation

The LA requires that inertia be weak and the film be thin. Estimating the material derivatives (describing inertia) in the Navier–Stokes Eqs. 4–5, one can deduce that inertia is small if

$$\frac{\varepsilon}{\alpha} \ll 1 \tag{16}$$

(it can be shown that ε/α is, essentially, the Reynolds number). Then, recalling how the film thickness was scaled [see (3)], one can write the condition that the film be thin as

$$\alpha \ll 1. \tag{17}$$

The LA also requires that the slope of the free surface relative to the cylinder wall be small. Recalling again non-dimensionalization (2–3), one can see that this requirement amounts to

$$\alpha\left|\frac{\partial h}{\partial\theta}\right| \ll 1. \tag{18}$$

Assuming (16–18), [2] (see also [11,12]) reduced Eqs. 4–7, 13–15 to

$$\frac{\partial}{\partial t}\left(h - \tfrac{1}{2}\alpha h^2\right) + \frac{\partial}{\partial\theta}\left[h - \tfrac{1}{3}h^3\cos\theta + \alpha\left(\tfrac{1}{2}h^4\cos\theta - \tfrac{1}{2}h^2 + \tfrac{1}{3}h^3\frac{\partial h}{\partial\theta}\sin\theta\right)\right] = \mathrm{O}(\varepsilon, \alpha^2, \gamma\alpha^3). \tag{19}$$

We are interested in steady flows. Assuming in (19) $\partial h/\partial t = 0$ and omitting also the small terms, we obtain

$$h - \tfrac{1}{3}h^3\cos\theta + \alpha\left(\tfrac{1}{2}h^4\cos\theta - \tfrac{1}{2}h^2 + \tfrac{1}{3}h^3\frac{\mathrm{d}h}{\mathrm{d}\theta}\sin\theta\right) = Q, \tag{20}$$

where Q is a constant of integration (physically, it represents the dimensionless flux of liquid along the circumference of the cylinder).

3 The results

Following most studies of rimming flows (including most references cited in this article), we shall employ assumptions (16–17). We shall also distinguish two regimes: $\gamma \ll 1$, for which surface tension is fully negligible, and; $\gamma \sim 1$, for which capillary effects are important in the shock region but negligible elsewhere.

3.1 The leading-order lubrication solution

In the lubrication limit (16–17), [2,3] have shown that rimming flows with shocks correspond to

$$Q = \tfrac{2}{3}. \tag{21}$$

Thus, for $\alpha \to 0$, Eqs. 20–21 reduce to a cubic equation [1],

$$h - \tfrac{1}{3}h^3 \cos\theta = \tfrac{2}{3}. \tag{22}$$

It can be shown that, for $\theta \in \left(-\pi, -\frac{1}{2}\pi\right)$ and $\theta \in \left(\frac{1}{2}\pi, \pi\right)$, Eq. 22 admits a single positive root and, for $\theta \in \left(-\frac{1}{2}\pi, \frac{1}{2}\pi\right)$, two positive roots. Accordingly, a shock solution is described by Benjamin et al. [2] and O'Brien and Gath [3]

$$h = \begin{cases} \text{the only positive root of (22)} & \text{if } \theta \in \left[-\pi, -\frac{1}{2}\pi\right], \\ \text{the smaller positive root of (22)} & \text{if } \theta \in \left(-\frac{1}{2}\pi, \theta_s\right), \\ \text{the larger positive root of (22)} & \text{if } \theta \in [\theta_s, 0], \\ \text{the smaller positive root of (22)} & \text{if } \theta \in \left(0, \frac{1}{2}\pi\right), \\ \text{the only positive root of (22)} & \text{if } \theta \in \left[\frac{1}{2}\pi, \pi\right]. \end{cases} \tag{23}$$

This solution involves a discontinuity at $\theta = \theta_s$ (see Fig. 1c).

Note that the volume of the liquid in the cylinder can be characterized by

$$V = \int_0^{2\pi} h \, \mathrm{d}\theta.$$

For solution (23), V depends on θ_s and varies within the limits

$$V_1 \le V < V_2,$$

where $V_1 \approx 4.44$ and $V_2 \approx 6.93$ correspond to $\theta_\mathrm{s} \to 0$ and $\theta_\mathrm{s} \to -\frac{1}{2}\pi$, respectively. Note also that Eq. 22 has no solutions with $V > V_2$.

3.2 The shock region

It is clear that, in the vicinity of the shock, the derivative in Eq. 20 cannot be omitted and, thus, the truncated Eq. 22 is invalid. The full Eq. 20 is not valid either, as a simple estimate shows that the applicability condition (18) does not hold near the shock. Thus, the LA [which was used to derive (20)] is invalid.

To derive a consistent equation describing the shock, we need to re-scale the azimuthal coordinate θ to the anticipated width of the jump ($\sim\alpha$) and, accordingly, the curvature of the free surface. Furthermore, the radial and azimuthal velocity near the jump should be comparable—hence, the former should be scaled up [recall that, in the original non-dimensionalization (3), v was scaled down by a factor of α]. Finally, the time derivative can be retained in the governing equations only if the time variable is re-scaled as well. Overall, we have

$$x = \frac{\theta - \theta_\mathrm{s}}{\alpha}, \qquad C_\mathrm{inner} = \alpha^2 C, \qquad v_\mathrm{inner} = \alpha v, \qquad t_\mathrm{inner} = \frac{t}{\alpha}. \tag{24}$$

Re-writing Eqs. 4–7, 11, and 13–15 in terms of the new variables, omitting the subscript $_\mathrm{inner}$, taking into account that $\varepsilon \ll \alpha \ll 1$, and assuming that γ may be O(1), we obtain, to leading order,

$$\frac{\partial p}{\partial x} = -\cos\theta_\mathrm{s} + \frac{\partial^2 u}{\partial x^2} + \frac{\partial^2 u}{\partial y^2}, \qquad \frac{\partial p}{\partial y} = \sin\theta_\mathrm{s} + \frac{\partial^2 v}{\partial x^2} + \frac{\partial^2 v}{\partial y^2}, \tag{25}$$

$$\frac{\partial u}{\partial x} + \frac{\partial v}{\partial y} = 0, \tag{26}$$

$$u = 1, \qquad v = 0 \qquad \text{at } y = 0, \tag{27}$$

$$-\left(2\frac{\partial u}{\partial x} - p - \gamma C\right)\frac{\partial h}{\partial x} + \frac{\partial u}{\partial y} + \frac{\partial v}{\partial x} = 0 \qquad \text{at } y = h, \tag{28}$$

$$-\left(\frac{\partial u}{\partial y} + \frac{\partial v}{\partial x}\right)\frac{\partial h}{\partial x} + 2\frac{\partial v}{\partial y} - p - \gamma C = 0 \qquad \text{at } y = h, \tag{29}$$

$$C = \left[1 + \left(\frac{\partial h}{\partial x}\right)^2\right]^{-3/2} \frac{\partial^2 h}{\partial x^2}, \tag{30}$$

$$\frac{\partial h}{\partial t} + u\frac{\partial h}{\partial x} - v = 0 \quad \text{at } y = h. \tag{31}$$

To match the solution of (25–31) to the outer solution (23), we require

$$h \to h_\pm \quad \text{as } x \to \pm\infty, \tag{32}$$

where the constants $h_\pm$ are the right/left limits of the outer solution near the shock, i.e.

$$h_\pm - \tfrac{1}{3}h_\pm^3 \cos\theta_s = \tfrac{2}{3}, \qquad h_+ > h_-. \tag{33}$$

Equations 25–33 describe a shock wave propagating down a plate which is moving upwards with the same velocity, so the absolute velocity of the wave is zero. Physically, the plate is tangent to the cylinder at the point where the outer solution has a discontinuity—thus, the plate is inclined at an angle $\theta_s + 90°$ to the horizontal. Observe also that, if $\gamma \sim 1$, surface tension contributes to Eqs. 28–29 and, thus, affects the shock.

In what follows, we shall need the far-field asymptotics of u, v, and p. To find them, assume that the unknowns in Eqs. 25–33 are independent of x and solve the resulting set of ordinary differential equations, which yields

$$\left.\begin{aligned} u &\to \left(\tfrac{1}{2}y^2 - yh_\pm\right)\cos\theta_s + 1, \\ v &\to 0, \\ p &\to (y - h_\pm)\sin\theta_s \end{aligned}\right\} \quad \text{as } x \to \pm\infty. \tag{34}$$

Unlike the LA (where the y-structure of the flow is resolved), Eqs. 25–33 involve two spatial variables and a free boundary, making them difficult to examine analytically. We integrated them numerically, using the finite-element solver available in the COMSOL Multiphysics package, version 3.4. The computations were carried out using the *Moving Mesh* mode incorporating the *Arbitrary Lagrangian-Eulerian* method, which allows the mesh to track the moving boundary. Within the domain, the motion of the nodes was unconstrained and computed by the software to optimize the element quality. Typically, the discretized problem included about 50,000 degrees of freedom, and the error of the numerical solution was approximately 10^{-3}.

We used the module for solving the Navier–Stokes equations and set the Reynolds number, Re, to be small—so the results obtained would provide an accurate approximation of the Stokes equations 25–26. Test simulations showed that $Re = 10^{-3}$ would provide the same accuracy as the COMSOL Multiphysics solver, but $Re = 10^{-5}$ was used as insurance.

The boundary conditions (34) were moved from infinity to $x = \pm X$, where X was large and such that a further increase by a factor of 2 would change the global characteristics of the solution by less than 10^{-3}.

For the initial condition, we generally used the steady-state solution for a case with similar parameter values. If such was not available, a smoothed step function was used for h, the hydrostatic pressure distribution for p, and the expressions predicted by the LA for u and v. Even though such conditions did not exactly satisfy the Stokes equations, they were automatically adjusted by the software and a self-consistent initial flow was generated. Then, the Navier–Stokes equations were integrated until a steady state was established.

Three main conclusions have been drawn, two of which apply to the case with zero surface tension, $\gamma = 0$, and one applying to the case $\gamma = \mathrm{O}(1)$.

(1) For $\gamma = 0$, for each θ_s from the range

$$-60° \lesssim \theta_s < 0°, \tag{35}$$

a steady solution exists. Examples can be seen in Fig. 2: observe that some solutions have oscillatory structure, which is particularly pronounced for the range $-30° \lesssim \theta_s < 0°$. In most of the remainder of the range (35), up to a certain threshold near $-60°$, the oscillations are also present, but they decay so quickly that they are not visible in Fig. 2.

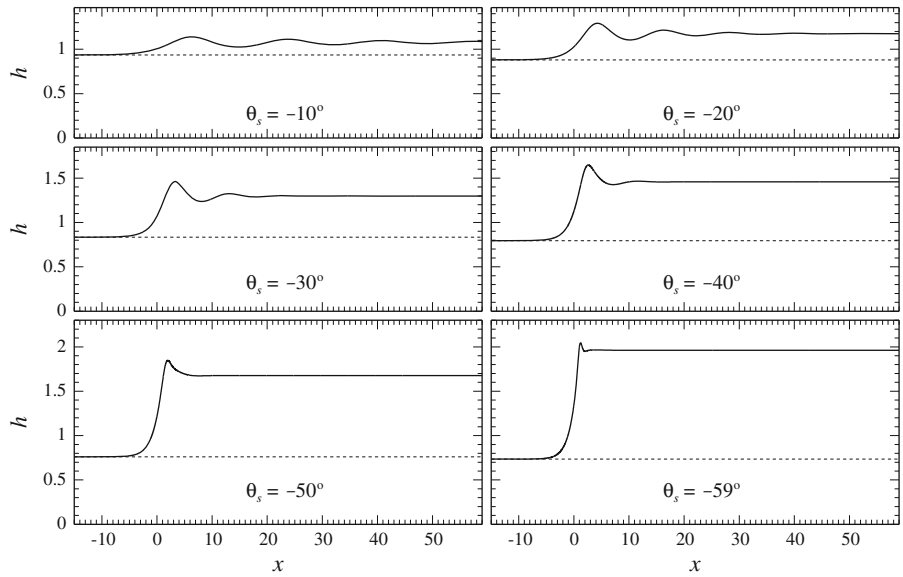

Fig. 2 Examples of smoothed-shock solutions of Eqs. 25–33 for $\gamma = 0$ and various θ_s. The *dotted line* corresponds to h_-

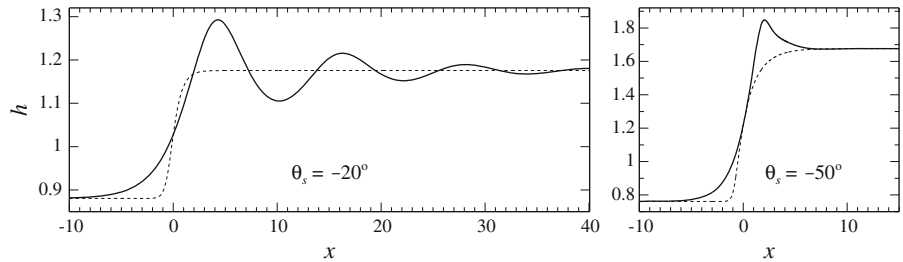

Fig. 3 Examples of smoothed-shock solutions of Eqs. 25–33 for $\gamma = 0$ (*solid line*), compared to those of the lubrication equation 36 (*dotted line*)

The oscillatory structure of the solution comes as a surprise, since the problem involves neither capillary nor gravity waves (the latter are eliminated by neglecting inertia in Eq. 25). The nature of the oscillations will be clarified in the next section.

It is instructive to compare the inner (smoothed-shock) solution derived through the Stokes equations to that obtained through the LA (20). To do so, re-write (20) in terms of the inner variables (24), omit the subscript inner, and keep the leading-order terms only, which yields

$$h - \tfrac{1}{3}h^3 \cos\theta_s + \tfrac{1}{3}h^3 \frac{\mathrm{d}h}{\mathrm{d}x} \sin\theta_s = Q. \tag{36}$$

This equation can be solved by separation of variables, but it is simpler to solve it numerically. Typical solutions are shown in Fig. 3 together with their analogs computed using the Stokes equations 25–33. Unlike the latter solutions, the former are strictly monotonic for all θ_s (which can also be verified analytically using Eq. 36). We conclude that, for rimming flows with shocks, the LA is neither quantitatively nor qualitatively correct.

(2) For $\gamma = 0$, no matter what initial conditions were used to simulate the range

$$-90^\circ < \theta_s \lesssim -60^\circ, \tag{37}$$

the shock always overturned (i.e. $\partial h/\partial x$ became infinite at some values of x and t). We conclude that set (25–33) with $\gamma = 0$ does not have steady solutions for range (37).

(3) We have also carried out simulations with $\gamma \neq 0$. Generally, if γ increases, the upper boundary of the non-existence region (37) decreases, and for $\gamma \gtrsim 0.23$ solutions exist for the whole allowable interval of θ_s, $(-90°, 0°)$. Thus, a sufficiently strong surface tension prevents all shocks from overturning.

To place this conclusion in a physical context, note that, in the experiments of Melo [13], the capillary coefficient varied between $\gamma \approx 0.04$ and $\gamma \approx 1.13$—but the results were presented mostly for $\gamma = O(1)$, and no shock overturning was reported. Thoroddsen and Mahadevan [14], in turn, presented experimental results for $0.008 \lesssim \gamma \lesssim 0.5$ and overturning was observed in some cases (which will be discussed in more detail in the next section). Finally, Tirumkudulu and Acrivos [6] carried out experiments with $0.3 \lesssim \gamma \lesssim 1$, and no overturning was observed.

4 Discussion

We shall now discuss the two most surprising features of the smoothed-shock (steady) solutions: the oscillatory structure observed for $\gamma = 0$ and the non-existence of solutions in a certain range of the parameter space.

4.1 Oscillations of smoothed-shock solutions

Some insight into the nature of the oscillations can be obtained by assuming that their amplitude is small (which it indeed is far from the shock region). In this case, the steady solution of set (25–33) can be represented in the form

$$\left.\begin{aligned} u = \bar{u}(y) + \tilde{u}(x, y), \quad v = \tilde{v}(x, y), \\ p = \bar{p}(y) + \tilde{p}(x, y), \; h = \bar{h} + \tilde{h}(x, y), \end{aligned}\right\} \tag{38}$$

where the variables with overbars/tildes describe the mean flow/small oscillations, respectively. The mean flow is given by (34) and can be re-written in the form

$$\bar{u} = \left(\tfrac{1}{2}y^2 - y\bar{h}\right)\cos\theta_s + 1, \qquad \bar{p} = \left(y - \bar{h}\right)\sin\theta_s, \tag{39}$$

where

$$\bar{h} = h_- \quad \text{or} \quad \bar{h} = h_+,$$

depending on which limit is considered, $x \to -\infty$ or $x \to +\infty$, respectively. Substituting (38–39) into Eqs. 25–33 and linearizing them, we obtain

$$\frac{\partial \tilde{p}}{\partial x} = \frac{\partial^2 \tilde{u}}{\partial x^2} + \frac{\partial^2 \tilde{u}}{\partial y^2}, \qquad \frac{\partial \tilde{p}}{\partial y} = \frac{\partial^2 \tilde{v}}{\partial x^2} + \frac{\partial^2 \tilde{v}}{\partial y^2}, \qquad \frac{\partial \tilde{u}}{\partial x} + \frac{\partial \tilde{v}}{\partial y} = 0, \tag{40}$$

$$\tilde{u} = 0, \qquad \tilde{v} = 0 \qquad \text{at } y = 0, \tag{41}$$

$$\frac{\partial \tilde{u}}{\partial y} + \tilde{h}\cos\theta_s + \frac{\partial \tilde{v}}{\partial x} = 0, \qquad 2\frac{\partial \tilde{v}}{\partial y} - \tilde{p} - \tilde{h}\sin\theta_s = 0 \qquad \text{at } y = \bar{h}, \tag{42}$$

$$\left(1 - \tfrac{1}{2}\bar{h}^2\cos\theta_s\right)\frac{\partial \tilde{h}}{\partial x} - \tilde{v} = 0 \qquad \text{at } y = \bar{h}. \tag{43}$$

We shall seek a solution of the form

$$\left.\begin{aligned} \tilde{u} = \hat{u}(y)\, \mathrm{e}^{-kx}, \; \tilde{v} = \hat{v}(y)\, \mathrm{e}^{-kx}, \\ \tilde{p} = \hat{p}(y)\, \mathrm{e}^{-kx}, \; \tilde{h} = \hat{h}\, \mathrm{e}^{-kx}, \end{aligned}\right\} \tag{44}$$

where k may be complex, in which case $\mathrm{Re}\, k$ and $\mathrm{Im}\, k$ represent the decay rate and wavenumber of the oscillations, respectively. Substitution of (44) into (40) yields three ordinary differential equations for $\hat{u}$, $\hat{v}$, and $\hat{p}$, which can readily be solved. Taking into account the no-slip/no-normal-velocity conditions (41), we obtain

$$\hat{u} = \frac{Aky\cos ky + \left(A + k^2 By\right)\sin ky}{k}, \tag{45}$$

$$\hat{v} = -Bky\cos ky + (B + Ay)\sin ky, \tag{46}$$

$$\hat{p} = -2Bk\cos ky + 2A\sin ky, \tag{47}$$

where A and B are undetermined constants. Substituting (44–47) into the free-surface boundary conditions (42–43), we obtain a set of three linear homogeneous equations for the constants A, B, and $\hat{h}$. This set has a non-trivial solution only if the determinant of the corresponding matrix is zero, yielding the following equation for k:

$$\left(1 - \tfrac{1}{2}\bar{h}^2\cos\theta_s\right)\left(k^2\bar{h}^2 - \cos^2 k\bar{h}\right) - \frac{\left(\sin 2k\bar{h} - 2k\bar{h}\right)\sin\theta_s}{4k^2} + \frac{\bar{h}^2\cos\theta_s}{2} = 0. \tag{48}$$

Thus, to determine the behavior of the solution as $x \to +\infty$, one needs to first solve Eq. 33 and find h_+. Then, assuming $\bar{h} = h_+$, one should solve Eq. 48 for k. Note that roots with $\mathrm{Re}\,k < 0$ should be discarded, as they make solution (44) grow as $x \to +\infty$.

It turns out that, for all θ_s, Eq. 48 has infinitely many roots with positive real parts. We shall denote these roots k_n ($n = 1, 2, 3\ldots$) and order them in such a way that

$$\mathrm{Re}\,k_{n+1} \geq \mathrm{Re}\,k_n. \tag{49}$$

Thus, the solution of the linearized set (40–43) is

$$\tilde{h} = \mathrm{Re}\sum_{n=1}^{\infty} C_n\,\mathrm{e}^{-k_n x}, \tag{50}$$

where C_n are arbitrary complex constants. Given (49), it follows from expression (50) that $\tilde{h}$ (and hence the full solution $\bar{h} + \tilde{h}$) oscillates as $x \to +\infty$ if and only if

$$\mathrm{Im}\,k_1 \neq 0.$$

Equation 48 was solved numerically, and the roots k_1, k_2, and k_3 are shown in Fig. 4 as functions of θ_s. Observe that, if

$$-58.5^\circ \lesssim \theta_s < 0^\circ, \tag{51}$$

k_1 has a non-zero imaginary part. Interval (51) covers almost all of region (35) where smoothed-shock solutions exist (for $\gamma = 0$)—hence, nearly all of them have oscillatory structure.

Equation 48 admits an infinite number of further roots, examples of which are shown in Fig. 5. All these roots have non-zero imaginary parts—but, since their real parts are significantly larger than $\mathrm{Re}\,k_1$, their contributions to solution (50) rapidly decay as $x \to +\infty$, so these roots yield negligible contributions to the sum in expression (50).

The values of k_1 computed using Eq. 48 corroborate the numerical solution of the full nonlinear Eqs. 25–33. For $\theta_s = -20^\circ$, for example, (48) yields

$$\frac{\pi}{\mathrm{Im}\,k_1} \approx 5.941. \tag{52}$$

This value is to be compared with the distances between two successive zeros of the function $h(x) - h_+$, where $h(x)$ is the steady solution of (25–33). For $\theta_s = -20^\circ$, these distances are

5.234, 6.572, 5.667, 6.130, 5.843, 6.005, 5.908

(this sequence does not include the three zeros nearest to the right-hand boundary of the computational domain, as these may have been affected by the fact that the boundary condition was moved from infinity to a finite position). It appears that the above sequence converges to the predicted value (52), as quantified by the value of approximately 5.943 given by a triple Shanks transformation [15] of the above sequence data.

We also examined Eq. 48 for $\bar{h} = h_-$. It turned out that, in this case, $\mathrm{Im}\,k_1 = 0$ for all θ_s. Thus, the smoothed-shock solutions of set (25–33) do not oscillate as $x \to -\infty$, which is indeed confirmed by the examples shown in Fig. 2.

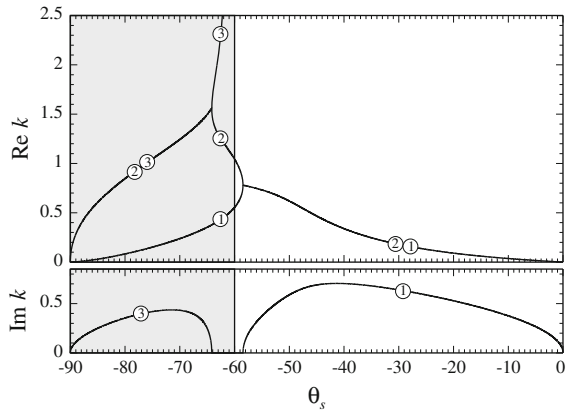

Fig. 4 The roots k_1, k_2, k_3 of Eq. 48 versus θ_s. The region where no smoothed-shock solutions exist is shaded. k_n are ordered in accordance with (49); it is also implied that $\mathrm{Im}\, k_2 = -\mathrm{Im}\, k_3$ for $\theta_s \in (-90°, -60°)$, $\mathrm{Im}\, k_2 = -\mathrm{Im}\, k_1$ for $\theta_s \in (-60°, 0°)$, and k_3 does not exist in the latter range

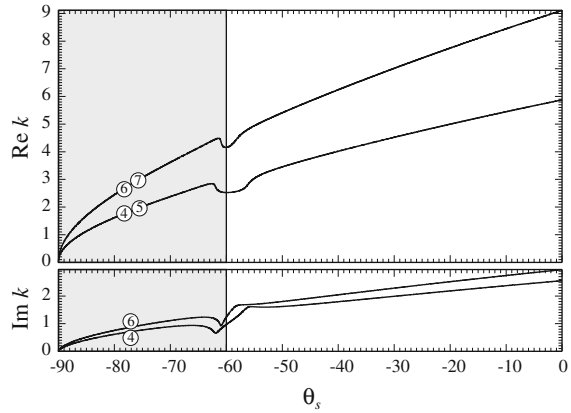

Fig. 5 The roots k_4, k_5, k_6, k_7 of Eq. 48 as functions of θ_s. The region where no smoothed-shock solutions exist is shaded. k_n are ordered in accordance with (49); it is also implied that $\mathrm{Im}\, k_5 = -\mathrm{Im}\, k_4$, $\mathrm{Im}\, k_7 = -\mathrm{Im}\, k_6$. Note that the *vertical scale* of this figure is larger than that of Fig. 4

Note that oscillatory solutions in models without an obvious wave mechanism have been observed before (see [16] and references therein). In those cases, the oscillations were caused by an interplay of dissipative and energy-generating effects (as in the Kuramoto–Sivashinsky equation examined in [16]).

Finally, note that surface tension may also give rise to oscillations near the shock (e.g., [5]), which may interfere with the oscillations examined above. The resulting pattern should depend on the position θ_s of the shock and the capillary parameter γ.

4.2 The non-existence of steady solutions in range (37)

The most important characteristic of overturning is the threshold value of θ_s, such that a steady solution exists for a larger θ_s but all solutions overturn for smaller values.

To approach this threshold more closely and, thus, improve the accuracy of its computation, the following method was employed. Initially, sufficiently strong surface tension was introduced to the problem, which stopped the overturning and gave rise to a steady smoothed-shock solution. Then surface tension was gradually phased out and, if overturning still occurred, we could reliably conclude that the threshold value of θ_s has been passed. If, on the other hand, the solution adjusted to the vanishing surface tension without overturning, we concluded that a steady solution still exists.

We assumed the following dependence of the capillary coefficient on time:

$$\gamma = \begin{cases} \gamma_0 & \text{if } 0 \le t \le T_1, \\ \gamma_0 \dfrac{T_2 - t}{T_2 - T_1} & \text{if } T_1 \le t \le T_2, \\ 0 & \text{if } T_2 \le t \le \infty. \end{cases} \tag{53}$$

The time T_1 was chosen sufficiently large that the solution would adjust to the constant capillary coefficient $\gamma = \gamma_0$, and an even larger T_2 was chosen so the solution would change adiabatically, adjusting to the intermediate values of $\gamma(t)$.

The results obtained by simulating the initial-value problem (25–33) with γ determined by (53) confirmed that, in the absence of surface tension, smoothed-shock solutions with $\theta_s \lesssim -60°$ do overturn. A typical steady solution for non-zero capillary coefficient and the corresponding overturning solution are shown in Fig. 6.

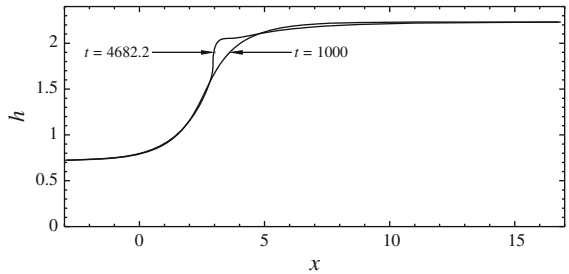

Fig. 6 Snapshots of the solution of equations (25–33) for $\theta_s = -65°$ and γ determined by (53) with $\gamma_0 = 0.5$, $T_1 = 1000$, $T_2 = 5000$. The curve for $t = 1000$ corresponds to $\gamma = 0.5$, and the curve for $t = 4682.2$ (the time of overturning) corresponds to $\gamma = 0.03178$

Our simulations also suggest that, for $\gamma = 0$, the theoretical threshold separating the ranges of overturning and steady solutions is very close, if not equal, to $\theta_s = -60°$. This issue, however, cannot be fully clarified, as solutions for $\theta_s \approx -60°$ turned out to be sensitive to the value of the Reynolds number used (recall that, instead of the Stokes equations, we simulated the Navier–Stokes equations with $\mathrm{Re} \ll 1$). In general, an increase in Re brings overturning forward, making it occur for larger values of θ_s. This conclusion agrees with one's intuition, as Re characterizes the inertia of the liquid, and inertial effects are conducive to overturning.

To understand why the case $\theta_s = -60°$ is special, note that, for this value of θ_s, Eq. 33 yields $h_+ = 2$. Then, formula (39) with $\bar{h} = h_+$ yields $u(h_+) = 0$, i.e., the liquid velocity at the free surface upstream from the shock vanishes. In can be further shown that, if $\theta_s < -60°$, then $u(h_+) < 0$—i.e., a near-surface layer upstream from the shock slides down—which is, intuitively, conducive to overturning.

It still remains to clarify what happens with rimming flows with $\theta_s \lesssim -60°$, for which no steady solution exists. One can conjecture that the shock region evolves periodically in this case: after the shock overturns, the free surface evens out—then a new shock forms and overturns—and so on. This scenario is difficult to simulate for the want of a numerical method capable of describing overturning beyond its initial stage, but there is some experimental evidence suggesting that our conjecture is correct. As observed in [14], the liquid on the rising side of the cylinder sometimes "sloshes to and fro". Furthermore, the parameter regime where such behavior occurs borders on the pool regime and, thus, corresponds to the shock located near the cylinder bottom—i.e., exactly where we predict overturning to occur.

Another piece of evidence supporting and complementing our results can be extracted from the experimental study of (non-rotating) flows down an inclined channel with a wavy bottom [17]. Even though the uneven bottom and the absence of rotation hinder quantitative comparisons with our work, it is worth mentioning that Wierschem and Aksel [17] observed steady shocks, as well as "periodic switching" between shocks and other flow types. Interestingly though, Wierschem and Aksel [17] also observed steady three-dimensional structures ("surface rollers"), which is an alternative scenario to the non-steady evolution reported in [14].

Full clarity in this issue, however, can only be achieved through a more detailed experiment specifically targeting overturning shocks in a rotating cylinder.

4.3 Applicability of the results obtained

Observe that, when $\theta_s \to -90°$, Eq. 33 yields

$$h_- \to Q + \mathrm{O}(\cos\theta_s), \qquad h_+ \to \left(\frac{3}{\cos\theta_s}\right)^{1/2} + \mathrm{O}(1).$$

Recalling how h was scaled [see (3)], we conclude that the approximation of thin film (under which both inner and outer solutions were obtained) holds only if

$$\cos\theta_s \gg \alpha^2. \tag{54}$$

Furthermore, as $\theta_s \to -90°$, it can be deduced from Eqs. 25–33 (by re-scaling them and balancing various terms to make the resulting set consistent) that the shock width grows as $O[(\cos\theta_s)^{-3/2}]$. Thus, recalling how x was scaled [see (24) and (2)], we conclude that the cylinder curvature can be neglected only if

$$\cos\theta_s \gg \alpha^{2/3}. \tag{55}$$

This condition is more restrictive than (54) and, hence, should be viewed as the validity criterion of our results. It suggests that the left boundary of the non-existence interval (37) is determined with an accuracy of $O(\alpha^{2/3})$.

Thus, in principle, solutions with a maximum near $\theta = -90°$ may exist. They should be viewed as marginal between shock and pool solutions, as the main bulk of liquid in this case pools very close to the cylinder bottom.

4.4 Comparison with the results of [6,7]

In [7], shock and pool solutions were computed using Eq. 20 and compared with those obtained through a phenomenological "modified lubrication equation" (MLE). In an earlier paper, [6], numerical solutions of the MLE were compared to those of the exact Navier–Stokes equations and experimental results of [13]. Eventually, Tirumkudulu and Acrivos [6] and Acrivos and Jin [7] concluded that, despite the fact that (20) was derived under the LA (which is, strictly speaking, inapplicable near the shocks and pools), its solution agrees well with the exact one. However, Tirumkudulu and Acrivos [6] and Acrivos and Jin [7] reported neither oscillating nor overturning shock waves.

In order to resolve the apparent discrepancy between Tirumkudulu and Acrivos [6], Acrivos and Jin [7], and this study, observe that the former papers illustrate their conclusions with the following examples:

I. $V = 14.95$, $\alpha = 0.0341$,
II. $V = 10.02$, $\alpha = 0.0376$,
III. $V = 6.22$, $\alpha = 0.0568$,
IV. $V = 5.78$, $\alpha = 0.0707$,

which correspond to their Figs. 3, 4, 5, and 6, respectively. One can see that, in cases I–II, V exceeds the threshold value of $V_2 \approx 6.93$ and, thus, these are actually pool (not shock) solutions. The remaining two cases appear to formally be shock solutions, with

III. $\theta_s \approx -87.3°$,
IV. $\theta_s \approx -82.1°$.

If, however, one estimates

III. $\cos\theta_s \approx 0.047$, $\alpha^{2/3} \approx 0.148$,
IV. $\cos\theta_s \approx 0.137$, $\alpha^{2/3} \approx 0.171$,

one can see that cases III–IV do not satisfy condition (55) and, thus, should be viewed as marginal between pool and shock solutions. We conclude that the numerical evidence supplied in [6,7] is not relevant to this article (which deals with shocks).

To test our results, we computed the solution of the Stokes equations for the cylindrical geometry and for several small values of α (again, using the COMSOL Multiphysics). As expected, if the liquid net mass was such that $-90° \lesssim \theta_s < -60°$, the corresponding shock wave overturned and no steady solution was found.

If, however, θ_s was sufficiently small, the flow would evolve toward a steady shock wave with oscillations—as illustrated in the upper panel of Fig. 7. This numerical solution was compared to the composite asymptotic one derived from the outer solution (23) and the inner solution computed using Eqs. 25–33. One can see that the latter provides a good approximation of the former near the shock, but the two solution do not agree well in a transitional region between the inner and outer zones.

For larger θ_s, as expected, oscillations of the solution are less visible—as illustrated in the lower panel of Fig. 7. Figure 7 also suggests that non-oscillating solutions are better approximated by the composite asymptotic solutions than the oscillating ones.

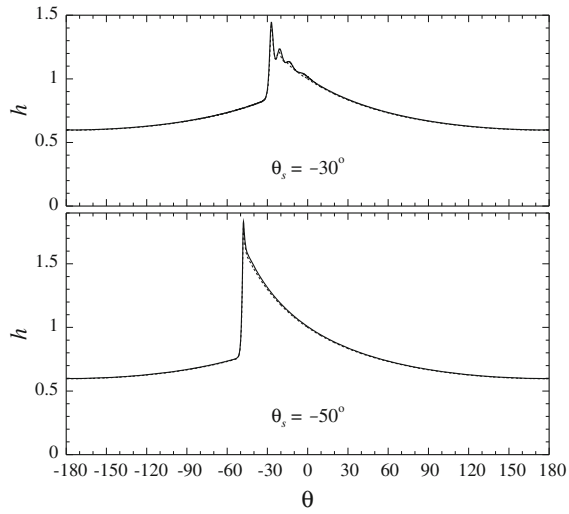

Fig. 7 Steady flows in a cylinder, for $\gamma = 0$ (no surface tension), $\alpha = 0.01$, and $\theta_s = -30°, -50°$. The solution of the Stokes equations and the composite asymptotic solution are shown by the *solid* and *dotted lines*, respectively

5 Summary and concluding remarks

In this study, we have examined rimming flows for which the leading-order LA predicts a discontinuity (shock) forming on the rising side of the cylinder. We have demonstrated that the shock region should be modeled by the full Stokes equations, resulting in a smooth solution.

Several features of the smoothed-shock solutions have been observed:

- In the absence of surface tension, a steady solution exists only if the shock is located in the two upper thirds of the fourth quadrant (i.e., for $-60° \lesssim \theta_s < 0°$).
- For most of this range (i.e., for $-58.5° \lesssim \theta_s < 0°$), the free surface upstream from the shock oscillates in space.
- For shocks located in the range $-90° \lesssim \theta_s < -60°$, no solution exists as all initial conditions overturn (unless surface tension is taken into account).
- If surface tension is taken into account, the region where solutions overturn contracts. If $\gamma \gtrsim 0.23$ [where γ is determined by (1)], solutions exist for all $\theta_s \in (-90°, 0°)$.

Note that all of the above features can be observed in smoothed-shock solutions describing liquid films flowing down an inclined plate. These are described by almost the same set of equations as those for the shock region of a rimming flow. There is one difference, however: to model the former problem, one should replace Eq. 33 for $h_\pm$ with

$$h_\pm - \tfrac{1}{3}h_\pm^3 \cos\theta_s = Q, \qquad h_+ > h_-,$$

where the dimensionless flux Q is a constant such that $0 < Q \leq \frac{2}{3}$.

Thus, mathematically, the inner (smoothed-shock) solution examined in this article is a particular case (for $Q = \frac{2}{3}$) of the more general problem of films on an inclined plate examined in [18].[2] Physically, however, this particular case is important (as it describes rimming flows) and, thus, deserves to be explored in detail.

Acknowledgments This study was supported by the Science Foundation Ireland through RFP Grant 08/RFP/MTH1476 and the Mathematics Application Consortium for Science and Industry (Grant 06/MI/005). We are also grateful to the referees, whose comments encouraged us to improve our work.

[2] Note that, the non-dimensional flux q of [18] is related to our Q by $q = Q\,(\cos\theta_s)^{1/2}$. Thus, this result is a particular case of [18] for $q = 2\,(\cos\theta_s)^{1/2}/3$.

References

1. Moffatt HK (1977) Behaviour of a viscous film on the outer surface of a rotating cylinder. J Méc 16:651–674
2. Benjamin TB, Pritchard WG, Tavener SJ (1993) Steady and unsteady flows of a highly viscous liquid inside a rotating horizontal cylinder. Report no. AM 122, Department of Mathematics, Penn State University (can be obtained from the authors of the present paper on request)
3. O'Brien SBG, Gath EG (1998) The location of a shock in rimming flow. Phys Fluids 10:1040–1042
4. Ashmore J, Hosoi AE, Stone HA (2003) The effect of surface tension on rimming flows in a partially filled rotating cylinder. J Fluid Mech 479:65–98
5. Benilov ES, Benilov MS, O'Brien SBG (2008) Stability of regularized shock solutions, with applications to rimming flows. J Eng Math 63:197–212
6. Tirumkudulu M, Acrivos A (2001) Coating flows within a rotating cylinder: lubrication analysis, numerical computations, and experimental measurements. Phys Fluids 13:14–19
7. Acrivos A, Jin B (2004) Rimming flows within a rotating horizontal cylinder: asymptotic analysis of the thin-film lubrication equations and stability of their solutions. J Eng Math 50:99–121
8. Benilov ES, Benilov MS, Kopteva N (2008) Steady rimming flows with surface tension. J Fluid Mech 597:91–118
9. Wilson SK, Hunt R, Duffy BR (2002) On the critical solutions in coating and rimming flow on a uniformly rotating horizontal cylinder. Q J Mech Appl Math 55:357–383
10. Hinch EJ, Kelmanson MA, Metcalfe PD (2004) Shock-like free-surface perturbations in low-surface-tension, viscous, thin-film flow exterior to a rotating cylinder. Proc R Soc Lond A 460:2975–2991
11. Benilov ES, O'Brien SBG (2005) Inertial instability of a liquid film inside a rotating horizontal cylinder. Phys Fluids 17:052106
12. Kelmanson MA (2009) On inertial effects in the Moffatt–Pukhnachov coating-flow problem. J Fluid Mech 633:327–353
13. Melo F (1993) Localized states in a film-dragging experiment. Phys Rev E 48:2704–2714
14. Thoroddsen ST, Mahadevan L (1997) Experimental study of coating flows in a partially-filled horizontally rotating cylinder. Exp Fluids 23:1–13
15. Shanks D (1955) Non-linear transformation of divergent and slowly convergent sequences. J Math Phys 34:1–42
16. Adams KL, King JR, Tew RH (2003) Beyond-all-orders effects in multiple-scales asymptotics: travelling-wave solutions to the Kuramoto-Sivashinsky equation. J Eng Math 45:197–226
17. Wierschem A, Aksel N (2004) Hydraulic jumps and standing waves in gravity-driven flows of viscous liquids in wavy open channels. Phys Fluids 16:3868–3877
18. Benilov ES, Lapin VN (2011) Shock waves in Stokes flows down an inclined plate. Phys Rev E 83:066321-1–066321-5